Int. J. Oral Maxillofac. Surg. 2024; xx: 1–9
https://doi.org/10.1016/j.ijom.2024.08.001, available online at https://www.sciencedirect.com

International Journal of Oral & Maxillofacial Surgery

Clinical Paper
Clinical Pathology

Dissecting the heterogeneity of craniofacial lesions in patients with fibrous dysplasia/ McCune–Albright Syndrome

N. Shah[a], L.A. Drubach[b], C. Berry[c], M. Mannstadt[d], Z.S. Peacock[e], J. Upadhyay[c,f], Craniofacial Fibrous Dysplasia Research Team[1]

[a]Department of Radiology, Brigham and Women's Hospital, Harvard Medical School, Boston, MA, USA; [b]Department of Radiology, Boston Children's Hospital, Harvard Medical School, Boston, MA, USA; [c]Department of Anesthesiology, Critical Care and Pain Medicine, Boston Children's Hospital, Harvard Medical School, Boston, MA, USA; [d]Endocrine Unit, Massachusetts General Hospital, Harvard Medical School, Boston, MA, USA; [e]Department of Oral and Maxillofacial Surgery, Massachusetts General Hospital, Harvard School of Dental Medicine, Boston, MA, USA; [f]Department of Psychiatry, McLean Hospital, Harvard Medical School, Belmont, MA, USA

N. Shah, L. A. Drubach, C. Berry, M. Mannstadt, Z. S. Peacock, J. Upadhyay: Dissecting the heterogeneity of craniofacial lesions in patients with fibrous dysplasia/McCune–Albright Syndrome. Int. J. Oral Maxillofac. Surg. 2024; xx: 1–9. © 2024 International Association of Oral and Maxillofacial Surgeons. Published by Elsevier Inc. All rights are reserved, including those for text and data mining, AI training, and similar technologies.

Abstract. Fibrous dysplasia/McCune–Albright Syndrome (FD/MAS) frequently involves the craniofacial skeleton. Craniofacial fibrous dysplasia lesions exhibit diverse imaging characteristics on multimodality evaluation, utilizing radiographs, computed tomography (CT), magnetic resonance imaging (MRI), and ^{18}F-sodium fluoride positron emission tomography (^{18}F-NaF PET). A multimodal imaging classification of craniofacial fibrous dysplasia lesions may offer clinical insights into the types of lesions that are (1) prone to progression, (2) amenable to intervention (i.e., pharmacological or surgical), or (3) associated with symptoms such as pain. In this prospective, preliminary single site study of 15 patients with FD/MAS, the heterogeneity of craniofacial lesions (N = 35) was assessed using a combination of ^{18}F-NaF PET, MRI, and CT. A k-means clustering algorithm was used to categorize lesions based on imaging characteristics. Clustering analysis revealed three types of lesion based on the magnitude of the regional ^{18}F-NaF standardized uptake values (SUV), signal intensities on T1-weighted and fluid-sensitive sequences, and appearance on CT (lucent, sclerotic, and/or ground glass). This preliminary study provides a foundation for future longitudinal natural history or treatment studies, where the prognostic value of baseline craniofacial fibrous dysplasia imaging characteristics and clinical symptomatology can be further evaluated.

Keywords: Craniofacial fibrous dysplasia; Positron-emission tomography; Magnetic resonance imaging; X-ray computed tomography; McCune-Albright Syndrome.

Accepted for publication 2 August 2024
Available online xxxx

Fibrous dysplasia (FD) is a rare genetic and non-inheritable skeletal disorder arising from a postzygotic, somatic missense mutation of the *GNAS* gene, which encodes the Gsα protein, a subunit of heterotrimeric G proteins[1,2].

[1] Craniofacial Fibrous Dysplasia Research Team: Hanne van der Heijden, Emma Golden, Anthony Westbrook, Stephan Voss, Neha Kwatra, Laura Romo, David Ebb, Leonard B. Kaban, Mariesa Cay, Alison M. Boyce.

 © 2024 International Association of Oral and Maxillofacial Surgeons. Published by Elsevier Inc. All rights are reserved, including those for text and data mining, AI training, and similar technologies.

The gain-of-function *GNAS* mutation results in the replacement of healthy bone tissue and marrow by pre-osteoblastic fibrous tissue, producing skeletal deformities and a lytic bone structure, increased propensity towards fracture, musculoskeletal weakness, and pain[3,4]. Lesions or skeletal damage may be solitary (monostotic FD) or multifocal (polyostotic FD). A distinct diagnosis, McCune–Albright Syndrome (MAS), is characterized by FD in conjunction with endocrinopathies and hyperpigmented skin macules[5–7].

The axial, appendicular, and craniofacial skeleton may be affected in FD/MAS. Involvement of the appendicular skeleton and spine frequently manifests in bodily pain or gait disturbances, whilst craniofacial involvement may result in facial deformity, malocclusion, dental pathology, vision or hearing loss, orofacial pain, headaches, and/or migraine[8–13]. Most lesions in the craniofacial skeleton are present and detectable by the age of 3.4 years (90%), and no new lesions seem to occur after the age of 10 years[14]. Complications arising from craniofacial lesions are variable and highly specific to the region(s) affected. In the case of frontal, maxillary, or mandibular lesions, facial asymmetry is often observed, whereas temporal bone lesions may result in hearing loss[15,16]. If the skull base or sphenoid is affected, deformation of the optic canals can lead to visual impairments[15,17,18]. A recent study has demonstrated an imperfect relationship between the presence of trigeminal nerve compression or displacement by craniofacial FD lesions and patient self-reports of pain[19].

Craniofacial lesions usually grow gradually in childhood, often with rapid growth phases in early life and pre-pubertal adolescence[20]. In FD/MAS, lesion expansion and craniofacial deformities may also be exacerbated by growth hormone excess[21,22]. Lesions may develop cystic degeneration and have potential for malignant transformation[23]. The clinical management of craniofacial FD is primarily guided by symptoms. Aggressive, fast-growing, and very symptomatic craniofacial FD lesions may require pharmacological and/or surgical treatment and frequent monitoring. In cases where surgical contouring is required for aesthetic reasons, it is critical that the lesion is quiescent or slow-growing because of the frequent recurrence of the lesion after surgery. Methods that provide a detailed characterization of craniofacial FD lesions could help in the tailoring of treatment strategies for individual patients, as well as in identifying methods to monitor patients accurately and safely.

Craniofacial lesions tend to mineralize over time, making differentiation of fibrous tissue from normal bone during surveillance more challenging[24–26]. Sensitive imaging techniques are critical for detecting or predicting either the progression of disease (i.e., cystic degeneration or malignant transformation of mature lesions) or response to treatment. The current authors hypothesized that the properties of FD lesions could be categorized using a multimodal imaging approach that includes ^{18}F-sodium fluoride positron emission tomography (^{18}F-NaF PET/CT), magnetic resonance imaging (MRI), and computed tomography (CT)[27,28]. The aim of this pilot investigation was to classify craniofacial lesions in patients with FD/MAS based on imaging characteristics.

Materials and methods

Study design

This prospective, cross-sectional study was approved by the institutional review boards of Boston Children's Hospital (Ref. IRB-P00030755) and Massachusetts General Brigham (Ref. 2019P003403), and has been registered at clinicaltrials.gov (NCT04125862). FD/MAS patients were recruited via local physician referrals, the FD/MAS Alliance, and the National Institute of Dental and Craniofacial Research Natural History study (clinicaltrials.gov, NCT00001727). Eligible patients had a confirmed diagnosis of monostotic FD, polyostotic FD, or MAS and were willing to provide informed consent[4]. Diagnoses were verified by a review of the patients' medical and imaging records, including whole-body bone scan, craniofacial CT, or craniofacial MRI. All adult participants provided informed consent prior to study enrollment. For patients under 18 years of age, informed consent from the guardian and assent from the patient was required.

^{18}F-NaF PET/CT

^{18}F-NaF PET/CT was performed using a Siemens Biograph Vision system (Siemens, Erlangen, Germany) at Boston Children's Hospital. PET/CT was acquired approximately 30 min after intravenous administration of ^{18}F-NaF. A dosage of 60 μCi per kilogram of body weight was used, with a maximum dose of 4 mCi. Imaging was performed of the whole body, from the vertex of the skull through the feet. A low-dose, non-contrast CT was obtained during the scan session. No sedation was used.

MRI

Multiplanar multisequence MRI of the head was obtained using a Siemens 3T MRI scanner with a dedicated 64-channel head coil (MAGNETOM Prisma; Siemens, Erlangen, Germany) at McLean Hospital, Belmont, Massachusetts. MRI was performed prior to ^{18}F-NaF PET/CT. All sequences were obtained in the axial plane. Depending on the location and orientation of the lesion, coronal and sagittal orientations were added. No sedation was used.

The following sequences were applied: (1) magnetization-prepared rapid gradient echo (MPRAGE), with repetition time (TR) of 2.53 s and echo time (TE) of 3.3 ms (TE1), 6.93 ms (TE2), 8.79 ms (TE3), and 10.65 ms (TE4), GRAPPA = 2, and resolution of 1 mm^3. (2) T1-weighted (T1W), with TR of 628 ms, TE of 9.2 ms, and slice thickness of 3.0 mm. (3) T2-weighted (T2W), with TR of 3730 ms, TE of 123 ms, and slice thickness of 3.0 mm. (4) Short tau inversion recovery (STIR), with TR of 4000 ms, TE of 33 ms, and slice thickness of 3.5 mm. (5) Fluid-attenuated inversion recovery (FLAIR), with TR of 9000 ms, TE of 81 ms, and slice thickness of 4.0 mm.

Evaluation of ^{18}F-NaF PET, MRI, and CT

^{18}F-NaF PET examinations were reviewed on a dedicated nuclear medicine workstation (Hermes; Hermes Medical, Stockholm, Sweden) by board-certified nuclear medicine physicians (L.A.D., S.V., N.K.). Findings on ^{18}F-NaF PET were characterized by the degree of uptake of the lesions, measured by the maximum standardized uptake values (SUVmax). Lesions demonstrating a range of SUVmax values were selected. Sub-lesion SUVmax values were calculated for lesions that demonstrated visual differences in the intra-lesional SUVmax. The lesions selected on PET/

CT were subsequently correlated to MRI findings.

MRI and CT examinations were reviewed on a picture archiving and communication system (PACS) (Visage; Visage Imaging Inc., San Diego, CA, USA) by board-certified radiologists (N.S., L.R.). The lesion signal on MRI was characterized as homogeneous if the entire lesion demonstrated uniform signal intensity, or as heterogeneous if there were internal areas of varying signal intensities. Sub-lesion characterization was performed for lesions that demonstrated heterogeneous signal intensity. Signal characteristics of the lesions and sub-lesions were defined on T1W and fluid-sensitive sequences (T2W, STIR, or FLAIR). Signal intensity relative to skeletal muscle was recorded for each lesion and for sub-lesions where applicable. Signal intensity was defined as low if the signal intensity was lower than skeletal muscle, intermediate or hyperintense if the signal intensity was similar or slightly increased, respectively, when compared to skeletal muscle, or as fluid signal intensity if it was similar to cerebrospinal fluid. Sub-lesion characterization was performed similarly. Where contrast-enhanced MRI was available, the presence or absence of enhancement of the lesions/sub-lesions was noted.

On CT, lesion attenuation was classified as sclerotic, ground glass, or lucent. A sclerotic lesion was defined as a lesion with higher attenuation than the surrounding trabecular bone. A ground glass lesion was defined as a lesion with uniform hazy attenuation. A lucent lesion was defined as having a lower attenuation than the surrounding trabecular bone. Lesions demonstrating mixed attenuation were classified according to their major attenuation pattern.

Data analysis

The mean SUVmax for ^{18}F-NaF for each lesion in each single patient dataset was automatically determined using Hermes software. The qualitative assessment of MRI signal intensity of each lesion was determined using Visage. Principal component analysis (PCA) was then conducted on the radiological data (^{18}F-NaF SUVmax, T1W MRI, T2W MRI, and CT). A PCA approach was used to reduce dimensionality while retaining at least 80% of the total variance. Four principal components were used for the radiological dataset (Supplementary material Table S1). Manual one-hot encoding was utilized to transform categorical data from T1W and T2W MRI signal intensity and CT appearance (lucent, sclerotic, ground glass) into binary vectors for analysis (Supplementary material Table S2). Following PCA, *k*-means clustering was applied. PCA and *k*-means algorithms were implemented using scikit-learn's PCA and KMeans modules, respectively (https://scikit-learn.org). The *k*-means clustering algorithm, configured with a predetermined number of clusters ($k = 3$) established through exploratory analysis, partitioned the data in each dataset into three distinct categories based on feature similarity within each cluster. Characteristic features were analyzed within each cluster for clinical relevance within the cohort.

Results

Patient overview

Fifteen patients with FD/MAS and craniofacial lesions were evaluated. Fourteen were female and one was male, and their mean ± standard deviation (SD) age was 36.2 ± 16.0 years. None of the patients were on active antiresorptive treatments (i.e., bisphosphonates or denosumab) at the time of imaging or symptom evaluation. A total of 35 craniofacial FD lesions were identified among the 15 FD/MAS patients, in the following locations: 19 calvarial, seven skull base, two mandibular, three maxillary sinus, three maxillary bone, and one nasal choanal (Table 1).

^{18}F-NaF PET

CT attenuation-corrected ^{18}F-NaF PET was available for 14 patients (33 lesions) and showed a variable degree of lesion uptake (SUVmax range 3–52.6). Most craniofacial FD lesions were found to be in a highly active bone turnover state by ^{18}F-NaF PET.

MRI

The craniofacial FD lesions demonstrated heterogeneous imaging characteristics on MRI. On T1W imaging, 14 lesions (40%) demonstrated low signal intensity, 19 lesions (54.3%) demonstrated heterogeneous intermediate signal intensity, and two lesions (5.7%) demonstrated mixed intermediate and low signal intensity. On fluid-sensitive sequences (i.e., T2W MRI, STIR, and FLAIR), 24 lesions (73.5%) were heterogeneously intermediate to hyperintense, five lesions (11.8%) were low signal intensity, two lesions (5.9%) demonstrated central hyperintensity and peripheral intermediate signal intensity, and three lesions (8.8%) demonstrated hyperintense fluid signal intensity. One lesion was not included within the field of view on the fluid-sensitive sequences (patient 5, Table 1).

CT

Attenuation correction CT revealed variable attenuation, ranging from diffusely sclerotic, ground glass, to lucent lesions. Expansion of the affected craniofacial bones was present. No periosteal reaction, pathological fracture, or extra-osseous extension was noted. Four lesions (12.1%) were diffusely sclerotic, 12 lesions (36.4%) demonstrated diffuse ground glass attenuation, five lesions (15.2%) were lucent, seven lesions (21.2%) demonstrated primarily ground glass appearance with lucent sub-regions, four lesions (12.1%) demonstrated primarily lucent appearance with sclerotic sub-regions, and one lesion (3.0%) demonstrated all three attenuations. Two lesions were not included on the CT images.

Lesion categorization

PCA produced four principal components with a total variance of 82.2% (Supplementary material Table S1). The *k*-means clustering analysis on radiological data from 33 fibrous dysplasia lesions yielded three distinct clusters (Fig. 1, Supplementary material Table S2). Patient 15, who had two lesions, did not undergo ^{18}F-NaF PET and was not included in the analysis. Representative lesions characterized by ^{18}F-NaF PET, MRI, and CT from each of the three clusters are shown in Fig. 2.

Ten lesions were classified to cluster 0. The mean ± SD SUVmax for these FD lesions was 27.6 ± 16.5 (range 8.0–50.8). The lesions displayed intermediate signal intensity on TIW MRI and hyperintense signal intensity on T2W sequences, occasionally accompanied by internal intermediate signal intensity nodules. Lesions predominantly exhibited lucent attenuation on CT, with instances of mixed lucent and ground glass appearance.

Table 1. Craniofacial fibrous dysplasia lesion presentation on ^{18}F-NaF PET, non-contrast MRI, and CT.

Patient	Location	^{18}F-NaF SUVmax	T1W MRI or MPRAGE	T2W MRI, FLAIR, STIR	CT	Radiological cluster
1	Right temporal	14.8	Intermediate	Intermediate	Lucent + ground glass	2
	Skull base	43.3	Intermediate	Hyperintense	Lucent	0
	Right temporal inferior	6.9	Low	Low	Sclerotic	1
	Right mandible	47	Intermediate	Hyperintense	Lucent + ground glass	0
2	Right maxillary sinus	50.8	Intermediate	Hyperintense	Lucent + ground glass	0
	Mandible	32	Intermediate	Hyperintense	Lucent	0
3	Left maxillary sinus	40	Intermediate	Intermediate	Ground glass	2
4	Left temporal bone superior	9.2	Intermediate	Hyperintense	Lucent	0
	Left temporal bone squamous	Central: 9.5 Peripheral: 3	Low	Low	Lucent + sclerotic	1
	Skull base	34	Intermediate	Intermediate	Ground glass	2
5	Left maxilla	20.3	Low	-[a]	Ground glass	2
6	Left frontal	39	Intermediate	Intermediate	Lucent + sclerotic	1
	Skull base	21	Intermediate	Intermediate	Ground glass	2
7	Right maxilla	52.6	Intermediate	Intermediate	Lucent + sclerotic	1
	Right frontal central	14	Intermediate	Central hyperintense, nodule intermediate	Central lucent, nodule ground glass	0
	Right frontal posterior	19	Intermediate	Central hyperintense, nodule intermediate	Central lucent, nodule ground glass	0
	Right maxillary sinus	29	Intermediate	Low	Lucent + ground glass + sclerotic	1
8	Left temporal	20	Low	Intermediate	Sclerotic	1
	Skull base	28	Intermediate	Intermediate	Ground glass	2
	Left choana	35	Low	Low	Sclerotic	1
9	Left temporal	7.6	Intermediate	Intermediate	Ground glass	2
10	Left frontal lateral	28	Low	Hyperintense	Ground glass	2
	Skull base	46	Low	Intermediate	Ground glass	2
	Left frontal anterior	35.7	Low	Intermediate	Ground glass	2
	Midline occipital	36.1	Low	Intermediate	Lucent	1
11	Frontal bone	29	Low	Intermediate	Ground glass	2
12	Midline skull base	26	Intermediate	Hyperintense	Lucent + ground glass	0
	Right occipital	25	Low	Intermediate	Sclerotic	1
	Left temporal	28	Low	Intermediate	Lucent + sclerotic	1
13	Frontal right	8	Intermediate	Hyperintense	Lucent	0
	Frontal left	39	Low	Low	Ground glass	2
14	Right frontal	45	Intermediate	Intermediate	Ground glass	2
	Posterior midline calvarium	Central: 10 Peripheral: 27	Intermediate	Central hyperintense fluid signal intensity, peripheral intermediate	Central lucent peripheral ground glass	0
15	Right maxilla	-[b]	Low	Intermediate	(-[b])	NA
	Sphenoid	-[b]	Intermediate	Central hyperintense fluid signal intensity, peripheral intermediate	(-[b])	NA

18F-NaF, ^{18}F-sodium fluoride; CT, computed tomography; FLAIR, fluid-attenuated inversion recovery; MPRAGE, magnetization-prepared rapid gradient echo; MRI, magnetic resonance imaging; PET, positron emission tomography; SUVmax, maximum standardized uptake value; T1W, T1-weighted; T2W, T2-weighted; STIR, short tau inversion recovery.

[a]Lesion was outside the field of view.

[b]^{18}F-NaF PET/CT was not performed.

Ten lesions were classified to cluster 1. The mean ± SD SUVmax for these FD lesions was 28.1 ± 13.8 (range 6.9–52.6). The lesions primarily showed low signal intensity on T1W sequences and a mixture of low to intermediate signal intensity on T2W sequences. On CT, the lesions exhibited sclerotic attenuation with instances of mixed sclerotic and ground glass appearance.

Thirteen lesions were classified to cluster 2. The mean ± SD SUVmax for these FD lesions was 29.9 ± 11.6 (range 7.6–46). The lesions exhibited a mixed signal intensity ranging from low to intermediate on T1W sequences and predominantly intermediate signal intensity on T2W sequences, while having a ground glass appearance on CT.

A summary of cluster characteristics is shown in Table 2. Cluster 0 was uniquely characterized by lesions exclusively exhibiting intermediate T1 signal intensity, hyperintense T2 signal intensity, and a lucent attenuation on CT, while cluster 2 exclusively demonstrated a ground glass attenuation on CT. SUVmax did not vary significantly between clusters ($P = 0.914$).

Discussion

This exploratory study aimed to determine whether craniofacial lesions in patients with FD/MAS could be classified using multiple imaging modalities including ^{18}F-NaF PET, non-contrast enhanced MRI, and CT in conjunction

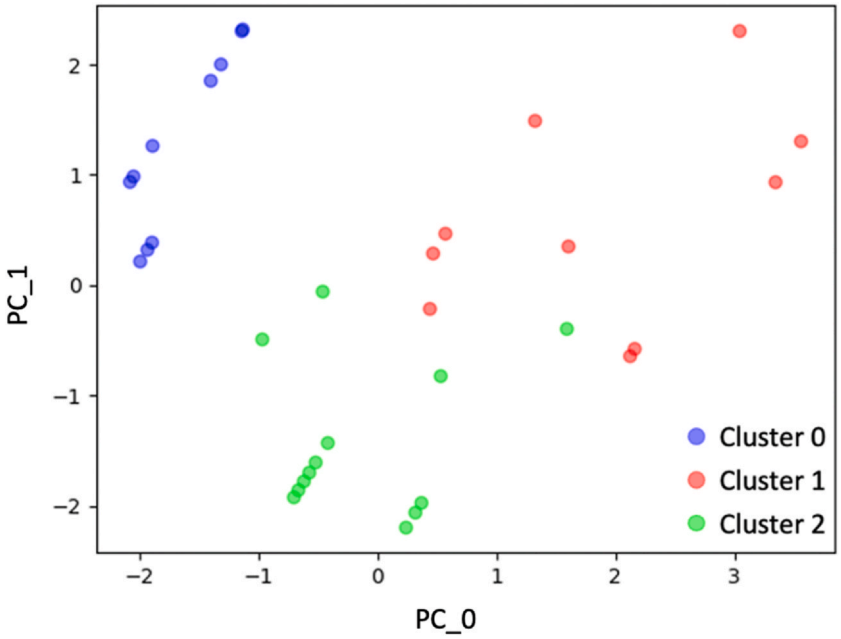

Fig. 1. *k*-means clustering analysis of radiological data. The scatter plot demonstrates *k*-means clustering of the radiological data from 33 craniofacial fibrous dysplasia lesions. Three clusters of lesions emerged based on ^{18}F-NaF SUVmax, T1W and T2W MRI signal intensity, and CT appearance (sclerotic, ground glass, or lucent). SUVmax, maximum standardized uptake value; T1W, T1-weighted; T2W, T2-weighted.

with *k*-means clustering analysis. Three distinct categories of craniofacial FD lesion were identified using the magnitude of regional ^{18}F-NaF uptake, signal intensities on T1W and fluid-sensitive sequences, and lesion attenuation on CT.

The results of this study support the variable imaging presentations of craniofacial FD lesions. In agreement with previous investigations, the current study confirms that ^{18}F-NaF PET/CT provides excellent information on the localization of high lesion activity (i.e., bone turnover and remodeling) and disease burden[29–31], and CT alone allows for accurate lesion identification and localization. However, there is cumulative ionizing radiation exposure from ^{18}F-NaF PET/CT and CT examinations performed at regular intervals. Classifying craniofacial FD lesions into distinct categories after an initial ^{18}F-NaF PET/CT evaluation could help predict lesion progression, allowing for interceptive treatment to prevent expansion or symptom development. Proper classification may also inform the clinician regarding the need for more frequent assessment or medical therapy. Routine surveillance with T1W MRI and fluid-sensitive sequences would eliminate the need for radiation, while still allowing for changes in size and appearance to be monitored. Contrast-enhanced MRI is likely unnecessary for routine surveillance, as pre-contrast T1W MRI and fluid-sensitive sequences effectively demonstrated lesion size and signal characteristics including cystic fibrous dysplasia lesions that are hyperintense on fluid-sensitive sequences.

T2W and STIR MRI sequences detected hyperintense or focally hyperintense intralesional regions in 12 lesions. In two patients (patients 13 and 14), the signal intensity approached that of cerebrospinal fluid, and SUVmax was low at below 15. These areas of hyperintensity and low bone turnover likely indicate a cystic region. The detection of cystic degeneration is important for clinicians to develop a treatment plan, as aneurysmal bone cyst-like changes can present unique challenges to surgical intervention[32].

Hyperintensity on fluid-sensitive sequences aligned with lesions appearing lucent or mixed lucent and ground glass on CT. On CT, the appearance of craniofacial FD lesions was found to be heterogeneous. Lesions were found to be of lucent, sclerotic, and/or ground glass attenuation, dependent on proportions of fibrous and osseous tissue. Ground glass attenuation was the most common lesion appearance on CT. Ground glass attenuation is caused by the presence of woven bone with variable mineralization. Lesions with ground glass and lucent CT appearances with hyperintensity on T2W MRI have fewer bony trabeculae[33]. Other factors such as cellularity, collagen, and cystic and hemorrhagic changes can also influence signal intensity on fluid-sensitive sequences[34].

^{18}F-NaF PET/CT and MRI have previously been employed to evaluate craniofacial lesions in FD/MAS patients. High variability of signal on both T2W MRI and contrast-enhanced images are seen, with T2W images more commonly showing hypointense or intermediate signal in craniofacial FD, whilst hyperintense lesions are more common in long bone FD[28]. Prior reports have demonstrated the clinical value of CT imaging in patients with craniofacial lesions. In a prior report of one FD patient with chronic headache, CT imaging allowed the detection and then treatment of a voluminous bilateral hyperdense expansive process in the frontal and ethmoid sinuses, and in a patient with acute decreased visual acuity, a CT scan revealed FD of the sphenoid bone and cystic changes leading to optic nerve compression[30,35]. The utility of ^{18}F-NaF PET/CT in linking the clinical endpoint with lesion characteristics has been demonstrated in a study showing that the total volume and activity of craniofacial lesions is associated with the lifetime and yearly number of craniofacial operations[30].

Multiple limitations for this study are considered. While no patients were undergoing antiresorptive treatments at the time of the study, some patients had a past history of denosumab use (a RANKL inhibitor). Denosumab can alter the appearance of FD lesions on radiographs, particularly in pediatric patients with FD/MAS[36,37]. Only two patients in the current study were under 18 years of age and neither had been treated previously with denosumab. Two individuals, patients 3 and 11, had received denosumab, with patient 3 first being treated at 13 years of age. Moreover, FD lesions in children have higher rates of bone metabolism that abate with age[38]. A study of pediatric patients could provide interesting insights into craniofacial lesion behavior during childhood, to predict outcomes of clinical interventions. Another potential study limitation is that there was only one male patient included, which differs from the reported sex distribution of

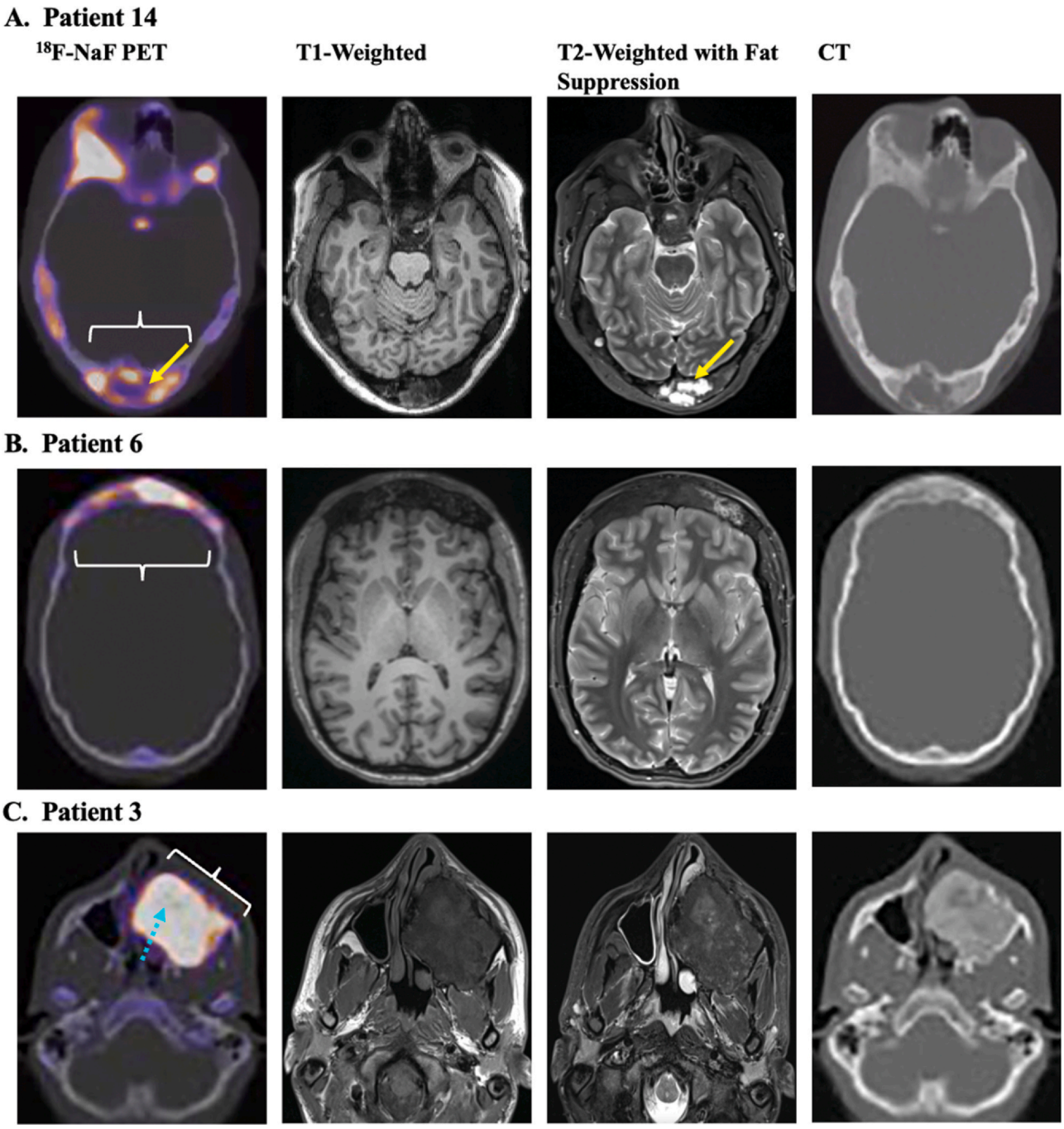

Fig. 2. Characterization of craniofacial fibrous dysplasia lesions with ^{18}F-NaF PET, non-contrast MRI, and CT. Multimodal imaging datasets are shown for three representative patients with craniofacial fibrous dysplasia from each radiological cluster (see Fig. 1). Each patient was prospectively evaluated with a combination of ^{18}F-NaF PET, T1W and T2W non-contrast MRI, and CT. (A) Patient 14 presented with multiple fibrous dysplasia lesions, including in the posterior midline calvarium. This lesion was categorized into radiological cluster 0. The centrally located region (solid yellow arrow) corresponded with a low ^{18}F-NaF SUVmax of 10, intermediate signal intensity on T1W MRI, hyperintense signal intensity on T2W MRI, and lucent appearance in CT. This region was suspected to be cystic in nature. (B) Patient 6 presented with a fibrous dysplasia lesion in the frontal bone slightly left of the midline (cluster 1). The lesion had high ^{18}F-NaF SUVmax of 39, intermediate signal intensity on T1W and T2W MRI, and primarily lucent appearance on CT with sclerotic sub-regions. (C) Patient 3 presented with a fibrous dysplasia lesion in the left maxillary sinus (cluster 2) with high ^{18}F-NaF uptake (SUVmax 40) and intermediate signal intensity on T1W and T2W MRI. On CT, the lesion demonstrated a ground glass appearance with a centrally located sub-region of decreased radiodensity (dotted blue arrow). SUVmax, maximum standardized uptake value; T1W, T1-weighted; T2W, T2-weighted.

Table 2. Summary of cluster characteristics.

	Cluster		
	0 ($n = 10$)	1 ($n = 10$)	2 ($n = 13$)
SUVmax (mean)	27.63	28.11	29.88
T1W MRI			
Low	0%	70%	46.2%
Intermediate	100%	30%	53.8%
T2W MRI			
Low	0%	40%	7.7%
Intermediate	30%	60%	76.9%
Hyperintense	100%	0%	7.7%
CT			
Lucent	100%	60%	7.7%
Ground glass	60%	10%	100%
Sclerotic	0%	90%	0%

CT, computed tomography; MRI, magnetic resonance imaging; SUVmax, maximum standardized uptake value; T1W, T1-weighted; T2W, T2-weighted.

59.4–68% female[39,40]. While the variability of FD lesions is well established, the causes of this heterogeneity are currently unknown. Lastly, additional longitudinal and prospective data are needed to link imaging and clinical phenotype, in order to determine the clinical significance of the subtypes described in the current study.

In conclusion, by employing a combination of imaging modalities and *k*-means clustering analysis, this study classified craniofacial fibrous dysplasia lesions into distinct subtypes. This investigation sets a foundation for future work where, for example, the progression or treatment response based on fibrous dysplasia lesion subtypes can be examined.

Ethical approval

Approved by the institutional review boards of Boston Children's Hospital (Ref. IRB-P00030755) and Massachusetts General Brigham (Ref. 2019P003403).

Funding

This research was funded by the MAYDAY Fund (PI: Dr. Upadhyay). The study sponsor had no role in the study design, data collection, data analysis, or data interpretation.

Data availability

The data that support the findings of this study are available from the corresponding author upon reasonable request.

Competing interests

Dr. Boyce has received support from Amgen Inc. (through the National Institute of Dental and Craniofacial Research) for an investigator sponsored study of denosumab treatment for fibrous dysplasia. The remaining authors declare no conflict of interest.

Acknowledgements. The authors thank the FD/MAS Alliance and FD/MAS Patient Registry for their support with patient outreach throughout the course of this study. The authors would also like to thank Dr. Henry Kronenberg for assistance with patient outreach.

Patient consent

All adult participants provided informed consent prior to study enrollment. For patients < 18 years of age, a parent or legal guardian provided informed consent and assent was obtained from the patient.

Trial registration

NCT04125862.

Appendix A. Supporting information

Supplementary data associated with this article can be found in the online version at doi:10.1016/j.ijom.2024.08.001.

References

1. Yang L, Wu H, Lu J, Teng L. Prevalence of different forms and involved bones of craniofacial fibrous dysplasia. *J Craniofac Surg* 2017;**28**:21–5. https://doi.org/10.1097/SCS.0000000000002830
2. Abdelkarim A, Green R, Startzell J, Preece J. Craniofacial polyostotic fibrous dysplasia: a case report and review of the literature. *Oral Surg Oral Med Oral Pathol Oral Radiol Endod* 2008;**106**:e49–55. https://doi.org/10.1016/j.tripleo.2008.03.023
3. Dumitrescu CE, Collins MT. McCune–Albright syndrome. *Orphanet J Rare Dis* 2008;**3**:12. https://doi.org/10.1186/1750-1172-3-12
4. Javaid MK, Boyce A, Appelman-Dijkstra N, Ong J, Defabianis P, Offiah A, Arundel P, Shaw N, Pos VD, Underhil A, Portero D, Heral L, Heegaard AM, Masi L, Monsell F, Stanton R, Dijkstra PDS, Brandi ML, Chapurlat R, Hamdy NAT, Collins MT. Best practice management guidelines for fibrous dysplasia/McCune–Albright syndrome: a consensus statement from the FD/MAS international consortium. *Orphanet J Rare Dis* 2019;**14**:139. https://doi.org/10.1186/s13023-019-1102-9
5. Alman BA, Greel DA, Wolfe HJ. Activating mutations of Gs protein in monostotic fibrous lesions of bone. *J Orthop Res* 1996;**14**:311–5. https://doi.org/10.1002/jor.1100140221
6. Shenker A, Weinstein LS, Sweet DE, Spiegel AM. An activating Gs alpha mutation is present in fibrous dysplasia of bone in the McCune–Albright syndrome. *J Clin Endocrinol Metab* 1994;**79**:750–5. https://doi.org/10.1210/jcem.79.3.8077356
7. Collins MT, Singer FR, Eugster E. McCune–Albright syndrome and the extraskeletal manifestations of fibrous dysplasia. *Orphanet J Rare Dis* 2012;**7**(Suppl. 1):S4. https://doi.org/10.1186/1750-1172-7-S1-S4
8. Golden E, van der Heijden H, Ren B, Randall ET, Drubach LA, Shah N, Cay M, Ebb D, Kaban LB, Peacock ZS, Boyce AM, Mannstadt M, Upadhyay J. Phenotyping pain in patients with fibrous dysplasia/McCune–Albright syndrome. *J Clin Endocrinol Metab* 2024;**109**:771–82. https://doi.org/10.1210/clinem/dgad589
9. Hartley I, Zhadina M, Collins MT, Boyce AM. Fibrous dysplasia of bone and McCune–Albright syndrome: a bench to bedside review. *Calcif Tissue Int* 2019;**104**:517–29. https://doi.org/10.1007/s00223-019-00550-z
10. Kelly MH, Brillante B, Collins MT. Pain in fibrous dysplasia of bone: age-related changes and the anatomical distribution

of skeletal lesions. *Osteoporos Int* 2008; **19**:57–63. https://doi.org/10.1007/s00198-007-0425-x

11. Spencer T, Pan KS, Collins MT, Boyce AM. The clinical spectrum of McCune–Albright syndrome and its management. *Horm Res Paediatr* 2019; **92**:347–56. https://doi.org/10.1159/000504802
12. Florez H, Peris P, Guañabens N. Fibrous dysplasia. Clinical review and therapeutic management. *Med Clin* 2016;**147**:547–53. https://doi.org/10.1016/j.medcli.2016.07.030
13. Majoor BCJ, Traunmueller E, Maurer-Ertl W, Appelman-Dijkstra NM, Fink A, Liegl B, Hamdy NAT, Sander Dijkstra PD, Leithner A. Pain in fibrous dysplasia: relationship with anatomical and clinical features. *Acta Orthop* 2019;**90**:401–5. https://doi.org/10.1080/17453674.2019.1608117
14. Hart ES, Kelly MH, Brillante B, Chen CC, Ziran N, Lee JS, Feuillan P, Leet AI, Kushner H, Robey PG, Collins MT. Onset, progression, and plateau of skeletal lesions in fibrous dysplasia and the relationship to functional outcome. *J Bone Miner Res* 2007;**22**:1468–74. https://doi.org/10.1359/jbmr.070511
15. Boyce AM, Brewer C, DeKlotz TR, Zalewski CK, King KA, Collins MT, Kim HJ. Association of hearing loss and otologic outcomes with fibrous dysplasia. *JAMA Otolaryngol Neck Surg* 2018; **144**:102–7. https://doi.org/10.1001/jamaoto.2017.2407
16. Ricalde P, Horswell BB. Craniofacial fibrous dysplasia of the fronto-orbital region: a case series and literature review. *J Oral Maxillofac Surg* 2001;**59**:157–67. https://doi.org/10.1053/joms.2001.20487
17. Lemme JD, Tucker-Bartley A, Drubach LA, Shah N, Romo L, Cay M, Voss S, Kwatra N, Kaban LB, Hassan AS, Boyce AM, Upadhyay J. Case report: a neuro-ophthalmological assessment of vision loss in a pediatric case of McCune–Albright syndrome. *Front Med* 2022;**9**:857079https://doi.org/10.3389/fmed.2022.857079
18. Boyce AM, Glover M, Kelly MH, Brillante BA, Butman JA, Fitzgibbon EJ, Brewer CC, Zalewski CK, Cutler Peck CM, Kim HJ, Collins MT. Optic neuropathy in McCune–Albright syndrome: effects of early diagnosis and treatment of growth hormone excess. *J Clin Endocrinol Metab* 2013;**98**:E126–34. https://doi.org/10.1210/jc.2012-2111
19. Golden E, Zhang F, Selen DJ, Ebb D, Romo L, Drubach LA, Shah N, O'Donnell LJ, Lemme JD, Myers R, Cay M, Kronenberg HM, Westin CF, Boyce AM, Kaban LB, Upadhyay J. Case report: the imperfect association between craniofacial lesion burden and pain in fibrous dysplasia. *Front Neurol* 2022; **13**:855157https://doi.org/10.3389/fneur.2022.855157
20. Lee JS, FitzGibbon EJ, Chen YR, Kim HJ, Lustig LR, Akintoye SO, Collins MT, Kaban LB. Clinical guidelines for the management of craniofacial fibrous dysplasia. *Orphanet J Rare Dis* 2012; **7**(Suppl. 1):S2. https://doi.org/10.1186/1750-1172-7-S1-S2
21. Lala R, Matarazzo P, Andreo M, Defilippi C, de Sanctis C. Impact of endocrine hyperfunction and phosphate wasting on bone in McCune–Albright syndrome. *J Pediatr Endocrinol Metab* 2002;**15**(Suppl. 3):S913–20.
22. Szwajkun P, Chen YR, Yeow VKL, Breidahl AF. The "Taiwanese Giant": hormonal and genetic influences in fibrous dysplasia. *Ann Plast Surg* 1998;**41**:75–80. https://doi.org/10.1097/00000637-199807000-00014
23. Qu N, Yao W, Cui X, Zhang H. Malignant transformation in monostotic fibrous dysplasia: clinical features, imaging features, outcomes in 10 patients, and review. *Medicine* 2015;**94**:e369https://doi.org/10.1097/MD.0000000000000369
24. Harris WH, Dudley HR, Barry RJ. The natural history of fibrous dysplasia. An orthopaedic, pathological, and roentgenographic study. *J Bone Joint Surg Am* 1962;**44-A**:207–33.
25. Weinstein LS, Shenker A, Gejman PV, Merino MJ, Friedman E, Spiegel AM. Activating mutations of the stimulatory G protein in the McCune–Albright syndrome. *N Engl J Med* 1991;**325**:1688–95. https://doi.org/10.1056/NEJM199112123252403
26. Parekh SG, Donthineni-Rao R, Ricchetti E, Lackman RD. Fibrous dysplasia. *J Am Acad Orthop Surg* 2004;**12**:305–13. https://doi.org/10.5435/00124635-200409000-00005
27. van der Bruggen W, Vriens D, Meier ME, Smit F, Winter EM, de Geus-Oei LF, Appelman-Dijkstra NM. Denosumab reduces lesional fluoride skeletal burden on Na[18F]F PET-CT in patients with fibrous dysplasia/McCune–Albright syndrome. *J Clin Endocrinol Metab* 2021; **106**:e2980–94. https://doi.org/10.1210/clinem/dgab212
28. Kinnunen AR, Sironen R, Sipola P. Magnetic resonance imaging characteristics in patients with histopathologically proven fibrous dysplasia—a systematic review. *Skeletal Radiol* 2020;**49**:837–45. https://doi.org/10.1007/s00256-020-03388-x
29. van der Bruggen W, de Geus-Oei LF, Appelman-Dijkstra NM, Vriens D. Considerations on bone volume normalization in quantifying skeletal burden in fibrous dysplasia using sodium fluoride PET/CT. *Eur J Nucl Med Mol Imaging* 2020;**47**:1351–2. https://doi.org/10.1007/s00259-020-04730-0
30. Ayadhi J, Youssef AB, Hamroun N. Dysplasie fibreuse ethmoïdo-frontale: à propos d'un cas [Fibrous dysplasia of the frontal and ethmoid sinuses: a case report]. *Pan Afr Med J* 2021;**38**:385. https://doi.org/10.11604/pamj.2021.38.385.27561. French.
31. van der Bruggen W, Hagelstein-Rotman M, de Geus-Oei LF, Smit F, Dijkstra PDS, Appelman-Dijkstra NM, Vriens D. Quantifying skeletal burden in fibrous dysplasia using sodium fluoride PET/CT. *Eur J Nucl Med Mol Imaging* 2020; **47**:1527–37. https://doi.org/10.1007/s00259-019-04657-1
32. Rau LH, Reinheimer A, Meurer MI, Marodin AL, Espezim CS, Klüppel LE, Dos Santos Vaz Fernandes PC, Rivero ERC. Fibrous dysplasia with secondary aneurysmal bone cyst—a rare case report and literature review. *Oral Maxillofac Surg* 2019;**23**:101–7. https://doi.org/10.1007/s10006-019-00741-w
33. Jee WH, Choi KH, Choe BY, Park JM, Shinn KS. Fibrous dysplasia: MR imaging characteristics with radiopathologic correlation. *AJR Am J Roentgenol* 1996; **167**:1523–7. https://doi.org/10.2214/ajr.167.6.8956590
34. Kushchayeva YS, Kushchayev SV, Glushko TY, Tella SH, Teytelboym OM, Collins MT, Boyce AM. Fibrous dysplasia for radiologists: beyond ground glass bone matrix. *Insights Imaging* 2018; **9**:1035–56. https://doi.org/10.1007/s13244-018-0666-6
35. Kıyat P, Top Kartı D, Esen Ö, Kartı Ö. Sphenoid bone dysplasia: a rare cause of compressive optic neuropathy mimicking glaucoma. *Turk J Ophthalmol* 2023; **53**:70–3. https://doi.org/10.5334/jbr-btr.467
36. Raborn LN, Burke AB, Ebb DH, Collins MT, Kaban LB, Boyce AM. Denosumab for craniofacial fibrous dysplasia: duration of efficacy and post-treatment effects. *Osteoporos Int* 2021;**32**:1889–93. https://doi.org/10.1007/s00198-021-05895-6
37. Wang HD, Boyce AM, Tsai JY, Gafni RI, Farley FA, Kasa-Vubu JZ, Molinolo

AA, Collins MT. Effects of denosumab treatment and discontinuation on human growth plates. *J Clin Endocrinol Metab* 2014;**99**:891–7. https://doi.org/10.1210/jc.2013-3081

38. Florenzano P, Pan KS, Brown SM, Paul SM, Kushner H, Guthrie LC, de Castro LF, Collins MT, Boyce AM. Age-related changes and effects of bisphosphonates on bone turnover and disease progression in fibrous dysplasia of bone. *J Bone Miner Res* 2019;**34**:653–60. https://doi.org/10.1002/jbmr.3649
39. Gokce E, Beyhan M. Radiological imaging findings of craniofacial fibrous dysplasia. *Turk Neurosurg* 2020;**30**:799–807. https://doi.org/10.5137/1019-5149.JTN.24627-18.2
40. Atalar MH, Salk I, Savas R, Uysal IO, Egilmez H. CT and MR imaging in a large series of patients with craniofacial fibrous dysplasia. *Pol J Radiol* 2015;**80**:232–40. https://doi.org/10.12659/PJR.893425

Correspondence to: Department of Anesthesiology
Critical Care and Pain Medicine
Boston Children's Hospital
Harvard Medical School
Boston
MA 02115
USA.
Tel:+1 917 736 1541.
E-mail:
jaymin.upadhyay@childrens.harvard.edu